Carbohydrate-attached Fullerene Derivative for Selective Localization in Ordered Carbohydrate-block-Poly(3-hexylthiophene) Nanodomains

Yoko Sakai-Otsuka, Yu Ogawa, Toshifumi Satoh, Wen-Chang Chen, Redouane Borsali

Carbohydrate-attached Fullerene Derivative for Selective Localization in Ordered Carbohydrate-*block*-Poly(3-hexylthiophene) Nanodomains

Yoko Sakai-Otsuka [a], Yu Ogawa [a], Toshifumi Satoh [b], Wen-Chang Chen [c], and Redouane Borsali [a, *]

[a] *Univ Grenoble Alpes, CNRS, CERMAV, F-38000 Grenoble, France*
[b] *Laboratory of Polymer Chemistry, Division of Applied Chemistry, Faculty of Engineering, Hokkaido University, N13W8, Kita-ku, Sapporo, 060-8628, Japan.*
[c] *Advanced Research Center for Green Materials Science and Technology, National Taiwan University, Taipei 10617, Taiwan*

** Corresponding Author*
Redouane Borsali – Univ Grenoble Alpes, CERMAV, CNRS, F-38000 Grenoble, France;
ORCID: https://orcid.org/0000-0002-7245-586X
Email Address: borsali@cermav.cnrs.fr

ABSTRACT

A carbohydrate-based fullerene derivative ($AcMal_7$-C_{61}) is designed, synthesized and applied to a lamellar-forming high-χ block copolymer system, poly(3-hexylthiophene)-*block*-peracetylated maltoheptaose (P3HT-*b*-$AcMal_7$), to actualize an ordered donor/acceptor (D/A) network. A well-defined D/A lamellar structure of the P3HT-*b*-$AcMal_7$:$AcMal_7$-C_{61} blend with sub-10 nm domain features is achieved upon thermal annealing. The $AcMal_7$-C_{61} molecules are localized in the phase-separated $AcMal_7$ nanodomains without causing the formation of fullerene crystals while maintaining the lamellar morphology up to 1:0.5 (D:A) blending ratio. The cross-sectional TEM observation and GISAXS measurement reveals that the P3HT-*b*-$AcMal_7$ tends to spontaneously organize into lamellar structures oriented perpendicular to the film surface at the air/film interface while the domain orientation at the bottom interface depends on the nature of the substrate.

Keywords:
Carbohydrate-based semiconducting block copolymers
Self-assembly
Nanostructured bulk heterojunction
Fullerene derivative
Organic photovoltaics

1. Introduction

Organic photovoltaics (OPVs) have been intensively studied in the past two decades in response to social demand for renewable energy technologies that can fulfill the needs for low-cost, light weight, and flexible energy devices (Dou et al., 2013). With extensive efforts on the device engineering and the material design, the power conversion efficiencies (PCEs) of single junction donor-acceptor (D/A) bulk-heterojunction (BHJ) solar cells have remarkably improved since the first demonstration of the BHJ concept in 1995 (Yu, Gao, Hummelen, Wudl, & Heeger, 1995).

Block copolymers have received significant attention in the area of organic optoelectronics because of their ability to self-organize into thermodynamically stable periodic nanostructures (Lee & Gomez, 2015; Segalman, McCulloch, Kirmayer, & Urban, 2009). Regioregular poly(3-hexylthiophene), P3HT, is one of the most employed *p*-type semiconducting polymers in the block copolymer systems. However, strong π-π interactions of the P3HT often prevents the microphase separation, eventually results in a randomly-oriented nanofibril structure (Boudouris, Frisbie, & Hillmyer, 2008; Iovu et al., 2007; Liu, Sheina, Kowalewski, & McCullough, 2002). Recently, we have reported the synthesis and morphological characterization of a carbohydrate-based block copolymer, poly(3-hexylthiophene)-*block*-peracetylated maltoheptaose (P3HT-*b*-AcMal$_7$). We revealed that, via the thermal annealing of the copolymer thin film, the P3HT-*b*-AcMal$_7$ can self-organize into a periodic lamellar structure having a sub-10 nm scale *d*-spacing. This periodicity is one of the smallest domain sizes ever reported in block copolymers containing crystalline π-conjugated polymer blocks (Sakai-Otsuka et al., 2017). This distinct morphology could be attained by the huge chemical and steric disparity (high χ) between the synthetic P3HT block and the naturally-derived carbohydrate block. Furthermore, an enhanced thermal stability of the P3HT crystalline structure was observed when the P3HT segments were confined in the phase-separated P3HT-*b*-AcMal$_7$ lamellae (Sakai-Otsuka et al., 2020).

While our previous works have highlighted the great potential of the P3HT-*b*-AcMal$_7$ as a system with an ideal morphology for OPV securing a high stability of the P3HT crystalline structure, the two following questions are yet to be answered: (i) how the semiconducting domains are organized in the film and (ii) how the ordered D/A nanostructures can be achieved by taking advantage of self-organization of the P3HT-*b*-AcMal$_7$. In this study, by addressing these questions, we aim at establishing a morphological control method best suited for our original P3HT-*b*-AcMal$_7$ system whilst providing the fine-tuned ideal D/A lamellar structures.

Controlling the morphology of photoactive layers remains a crucial challenge for performance enhancement of the OPVs. A perpendicularly-oriented periodic lamellar structure, in which electron donor and acceptor materials are alternately interpenetrating on the 10-nm length scale, has been recognized as an ideal geometry. This well-defined structure ensures (i) enlarged interface contact, (ii) optimal lateral domain size for exciton dissociation, (iii) the shortest charge transportation pathway in the vertical direction, and (iv) reduced charge trap sites (Coakley & McGehee, 2004; Shah & Ganesan, 2010). Although our previous study demonstrated the formation of the lamellar structures in the film, it was unclear how the semiconducting domains are organized with respect to the film surface.

Another issue is to achieve ordered D/A nanostructures by taking advantage of self-organization of the P3HT-*b*-AcMal$_7$. For instance, in case of a blend of P3HT and [6,6]-phenyl C_{61} butyric acid methyl ester ($PC_{61}BM$), small $PC_{61}BM$ molecules are easily diffused over the photoactive layer due to the lack of physical or chemical connections to the P3HT matrix. This instability causes inhomogeneous macrophase segregations of the blends, undesired crystallization or aggregation of $PC_{61}BM$, and eventually leads to the deterioration of device performance with long-term device operations or during post-annealing process. Several strategies have been implemented to localize fullerene-based *n*-type acceptors in a specific area of phase-separated block copolymer systems. Synthesizing D-A block copolymers consisting of a semiconducting donor polymer and another polymer bearing covalently attached acceptor

compounds is one of the promising approaches (Miyanishi, Zhang, Hashimoto, & Tajima, 2012; Miyanishi, Zhang, Tajima, & Hashimoto, 2010). Alternatively, non-covalent chemical interaction between acceptor materials and polymer blocks has also been exploited to immobilize the acceptors (Lin et al., 2012; Sary et al., 2010). Inspired by the latter approach, in this study, we designed a new fullerene derivative bearing $AcMal_7$ segment ($AcMal_7$-C_{61}) to immobilize the acceptor compounds in the $AcMal_7$ channel. We hypothesize that the $AcMal_7$-C_{61} would be excluded from P3HT domains during a post-thermal annealing process and predominately located within the phase-separated $AcMal_7$ domain owing to a total miscibility between the $AcMal_7$-C_{61} and $AcMal_7$ segments. Simultaneously, the $AcMal_7$-C_{61} is not expected to cause any microphase separation or crystallization of fullerenes in the $AcMal_7$ matrix because of a steric constraint of $AcMal_7$ moiety.

Here in, we present the synthesis of carbohydrate-based fullerene derivative $AcMal_7$-C_{61} and the reciprocal self-organization of the P3HT-*b*-$AcMal_7$:$AcMal_7$-C_{61} blends. The chemical structure of the $AcMal_7$-C_{61} was fully characterized by NMR, FT-IR, and mass spectroscopy. The validity of the approach was confirmed by investigating the morphology of the P3HT-*b*-$AcMal_7$:$AcMal_7$-C_{61} blends and crystalline structure of P3HT domains using transmission electron microscopy (TEM) and Wide-angle X-ray scattering (WAXS) analysis. In addition, an internal orientation of the self-assembled P3HT-*b*-$AcMal_7$ lamellar was investigated to gain further insight into the internal structure. TEM and grazing incidence small-angle X-ray scattering (GISAXS) measurements revealed that the P3HT-*b*-$AcMal_7$ tends to organize into perpendicularly-oriented lamellar structures relative to the film surface at the air/film boundary.

2. Experimental Section

2.1. Materials

[6,6]-Phenyl C_{61} butyric acid methyl ester ($PC_{61}BM$) was kindly gifted by PCAS (Longjumeau, France). Maltoheptaose was purchased from Nagase & Co., Ltd. (Japan). All other reagents

were purchased from Sigma-Aldrich and used as received without further purification unless otherwise specified. Reducing-end azide-functionalized peracetylated maltohepotaose ($AcMal_7$-N_3) and [6,6]-Phenyl C_{61} butyric acid ($PC_{61}BA$) were synthesized as previously reported (Hummelen et al., 1995; Sakai-Otsuka et al., 2017). Poly (3-hexylthiophene)-*b*-peracetylated maltoheptaose (P3HT-*b*-$AcMal_7$) was synthesized via copper(I)-catalyzed 1,3-dipolar azide-alkyne cycloaddition (CuAAC) click reaction of alkyne-functionalized regioregular P3HT (alkyne-P3HT) with the $AcMal_7$-N_3. The alkyne-P3HT was prepared by post-functionalization modification of Br/H-terminated P3HT via Stille coupling between Br-terminated polymer end with ethynyltributylstannane. Details of the synthesis and characterizations were described in the supporting information.

2.2. Instruments

^1H (400 MHz) and ^{13}C (100 MHz) NMR spectra were recorded using a Bruker Avance DRX 400 MHz. FT-IR spectra were recorded using a Perkin-Elmer Spectrum RXI FT-IR Spectrometer. TEM and electron diffraction (ED) measurements were carried out using CM200 Philips microscope (Thermo Fisher Scientific) operating at 200 kV equipped with a TVIPS F216 TemCam camera. Wide-angle X-ray scattering (WAXS) and Grazing incidence small-angle X-ray scattering (GISAXS) experiments were carried out on the BM02 beamline D2AM at the European Synchrotron Radiation Facility (ESRF, Grenoble, France). X-rays of 18 keV (λ = 0.6888 Å) with a spot size of 100 μm were used for WAXS. GISAXS was done with X-ray energy of 11 keV. Scattering patterns were recorded on two photon-counting pixel detectors (WOS and D5 from imXpad).

2.3. Synthesis of N-propargyl [6,6]-phenyl C_{61} butyramido (alkyne-$PC_{61}BAm$)

In a dry 100 mL three-neck round-bottom flask equipped with a reflux condenser, $PC_{61}BA$ (200 mg, 0.22 mmol, 1 equiv.) and thionyl chloride (4 mL) were introduced, and the mixture was

refluxed at 70 °C under an argon atmosphere until the FT-IR spectrum showed a complete disappearance of the peak at 1702 cm^{-1} corresponding to the C=O stretching vibration of carboxylic acid group in the $PC_{61}BA$. After the mixture was cooled to the room temperature, thionyl chloride was evaporated by vacuum pump. In another dry 50 mL flask, propargylamine (42.8 µL, 0.67 mmol, 3 equiv.), dry triethylamine (0.19 µL, 0.13 mmol, 6 equiv.) and THF (12 mL) were added and the solution was degassed by bubbling with argon for 5 min and stirred at room temperature. The solution of the propargylamine was transferred to the reaction mixture via syringe under argon atmosphere. The mixture was stirred at room temperature for 4h until the FT-IR spectrum showed a complete disappearance of the peak at 1793 cm^{-1} corresponding to the C=O stretching vibration of the carbonyl chloride group. The product was purified by precipitation in cold methanol and dried under reduced pressure to yield the *N*-propargyl [6,6]-phenyl C_{61} butyramido (alkyne-$PC_{61}BAm$) as a brown solid (88.5 mg, 43 %). ^{1}H-NMR (400 MHz, THF-d_8, δ): 8.01 (d, 2H, *o-H* aromatic), 7.53 (t, 2H, *m-H* aromatic), 7.44 (t, 1H, *p-H* aromatic), 7.34 (br, 1H, -N*H*-), 3.93 (m, 2H, -CH_2-C≡CH), 2.97 (m, 2H, -CH_2-CO-NH-), 2.53 (1H, -C≡C*H*), 2.32 (t, 2H, Ph-C-CH_2-), 2.16 (m, 2H, -CH_2-CH_2-CO-NH-); FT-IR (ATR): ν = 1646 cm^{-1} (C=O, butyramido); MALDI-TOF MS *m/z*: $[M - H]^-$ calcd for $C_{74}H_{14}NO$, 932.11; found, 932.93.

2.4. Synthesis of fullerene-attached AcMal$_7$(AcMal$_7$-C$_{61}$)

In a 250 ml flask, alkyne-$PC_{61}BAm$ (0.40 g, 0.43 mmol, 1 equiv.) and CuBr (91.6 mg, 0.64 mmol, 1.5 equiv.) were dissolved in THF (60 mL), degassed by bubbling with argon for 5 min, and stirred at room temperature. In another 100 mL flask, AcMal$_7$-N_3 (0.90 g, 0.43 mmol, 1 equiv.) and PMDETA (134 µL, 0.64 mmol, 1.5 equiv.) were dissolved in THF (20 mL), degassed by bubbling with argon for 5 min, and stirred at room temperature. The solution of AcMal$_7$-N_3 was transferred to the stirred solution of alkyne-$PC_{61}BAm$ via cannula under argon atmosphere. The reaction mixture was stirred at room temperature for 12h until the FT-IR

spectrum showed a complete disappearance of the signal corresponding to the azide group of AcMal$_7$-N$_3$. The reaction mixture was passed through a neutral alumina column to remove copper salt with a THF eluent. The crude product was purified by precipitation in cold methanol. The product was collected by centrifugation and dried under reduced pressure to give the AcMal$_7$-C$_{61}$ as a brown solid (0.76 g, 58 %). MALDI-TOF MS *m*/*z*: $[M + H]^+$ calcd for $C_{161}H_{131}N_4O_{58}$, 3036.75; found, 3036.98.

2.5. Ultrathin section preparation for TEM

An about 10 μm-thick film was prepared by drop casting from a concentrated THF solution of P3HT-*b*-AcMal$_7$ onto a PTFE substrate. After complete evaporation of the solvent, the obtained thick film was annealed at 220 °C for 10 min under vacuum to induce the microphase separation. A thin gold layer with a thickness of about 20 nm was sputtered on the film to distinguish the top side from the bottom side of the film. The thick film was then soaked in absolute ethanol for 1 hour to dehydrate and embedded in an epoxy resin (Embed-812). The hardened resin block was set on an ultramicrotome with the film plane being orthogonal to the sectioning direction. Ultrathin sections with a thickness of less than 100 nm were obtained using a 35° diamond knife with a clearance angle of 6°, and mounted onto carbon-coated copper grid.

3. Results and Discussion

3.1. Lamellae Orientation of P3HT-b-AcMal$_7$

The chemical structure and molecular properties of the P3HT-*b*-AcMal$_7$ used in this study are given in **Scheme 1** and **Table 1**, respectively. **Fig. 1a** shows a cross sectional TEM image of a thermally-annealed P3HT-*b*-AcMal$_7$ film in the vicinity of the interface of air (resin)/film surface. The film was prepared by a drop-casting on a PTFE-coated substrate with a thickness of *ca.* 10 μm. Interestingly, a lamellar structure oriented perpendicular to the surface was exclusively observed over more than 100 nm deep from the top surface while no preferential

orientation was observed at the bottom boundary (**Fig. S1**). This observation was further confirmed by the GISAXS measurement. **Fig. 1b** shows a two-dimensional GISAXS pattern of a thermally-annealed P3HT-*b*-AcMal$_7$ thin film with a film thickness of *ca*. 35 nm deposited on a silicon substrate. Clear spots parallel to the substrate corresponding to a *d*-spacing of 12.6 nm were observed, indicating the perpendicular orientation of lamellae to the film surface. Generally, if no treatment is applied, the perpendicular lamellar orientation of high-χ block copolymers cannot be spontaneously obtained due to an inherent strong repulsive force between the constituent blocks (Bates et al., 2012; Zhang et al., 2016). One of the two blocks that has a more favorable interaction with the surface tends to align along the surface boundary to minimize total interfacial energy, often resulting in the lamellar orientation parallel to the surfaces. Unlike this trend, the P3HT-*b*-AcMal$_7$ manifests a perpendicularly-oriented lamellae organization at the air boundary. While the reasons leading to this orientation are unknown for the moment, the P3HT-*b*-AcMal$_7$ has a potential to realize a desirable perpendicular lamellar organization across the entire film by tuning processing conditions or by using chemically and/or topographically modified substrates.

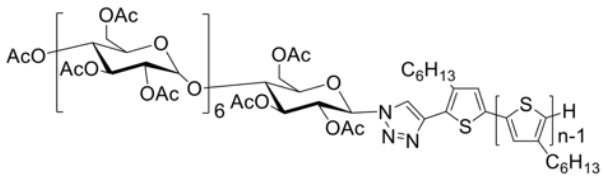

Scheme 1. Chemical structure of P3HT-*b*-AcMal$_7$.

Table 1. Molecular properties of the P3HT-*b*-AcMal$_7$ employed in this study

P3HT block						carbohydrate block		block copolymer	
$M_{n,SEC,P3HT}$[a)] [g mol^{-1}]	$M_{w,SEC,P3HT}$[a)] [g mol^{-1}]	$M_{p,MALDI,P3HT}$[b)] [g mol^{-1}]	$Đ_{,P3HT}$[a)]	% HT[c)]		M_{AcMal7}[d)] [g mol^{-1}]		$Đ_{,total}$[a)]	ϕ_{P3HT}[e)]
5670	6210	3682	1.07	> 95		2060		1.23	0.65

[a)]Number average molecular weight (M_n), weight average molecular weight (M_w), and polydispersity ($Đ$) determined by SEC in THF based on PS standards; [b)]molecular weight at the

peak maximum determined by MALDI-TOF MS; [c)]HT-HT regioregularity determined by ^{1}H NMR; [d)]molecular weight of carbohydrate block; [e)]volume fraction of P3HT in copolymers calculated by using density values 1.16 g cm^{-3} for P3HT and 1.20 g cm^{-3} for AcMal$_7$.

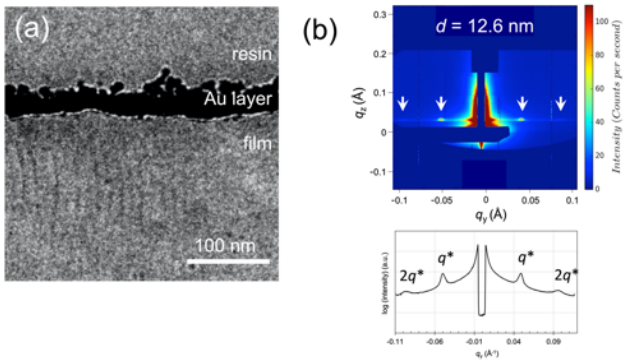

Fig. 1. (a) TEM image of the cross section of thermally annealed P3HT-*b*-AcMal$_7$ thick film in the vicinity of the film surface. (b) Two-dimensional GISAXS diffraction pattern of thermally annealed P3HT-*b*-AcMal$_7$ thin film.

3.2. Synthesis of AcMal$_7$-C$_{61}$

Fullerene-attached paracetylated maltoheptaose (AcMal$_7$-C$_{61}$) was synthesized as shown in **Scheme 2**. First, [6,6]-phenyl C$_{61}$ butyric acid (PC$_{61}$BA) was prepared via hydrolysis of PC$_{61}$BM following the literature procedure. (Hummelen et al., 1995) The PC$_{61}$BA was then reacted with thionyl chloride ($SOCl_2$) under reflux to afford reactive intermediate PC$_{61}$B-Cl. Note that, carbon disulfide (CS_2), which is known as one of the few good solvents for the PC$_{61}$BA, is generally used for the reaction (Hummelen et al., 1995; Miyanishi et al., 2012). However, it was found from our experiment that the reaction proceeded well in the solvent-free condition. The PC$_{61}$BA became soluble in the neat $SOCl_2$ over time and were completely converted to PC$_{61}$B-Cl within six hours. Considering the boiling points of $SOCl_2$ ($T_{b,\,SOCl2}$ = 75 °C) and CS_2 ($T_{b,\,CS2}$ = 46 °C), the absence of the CS_2 is more favorable to promote the reaction by heating near $T_{b,\,SOCl2}$. Subsequently, the PC$_{61}$B-Cl was reacted with propargylamine in the presence of dry trimethylamine to yield *N*-propargyl [6,6]-phenyl C$_{61}$ butyramido (alkyne-PC$_{61}$BAm) as brown solid. The resulting product was soluble in tetrahydrofuran (THF) and hardly soluble in toluene, chloroform, and *o*-dichlorobenzene. The FT-IR spectrum of the

alkyne-$PC_{61}BAm$ showed the -C=O stretching band of amide group at 1646 cm^{-1} but not the -C=O stretching band of the carbonyl chloride at 1793 cm^{-1}, indicating the complete conversion of the $PC_{61}B$-Cl to the corresponding amide (**Fig. 2**). ^1H NMR spectroscopy confirms the presence of the ethynyl group at 2.53 ppm (**Fig. S2**) and the full substitution of the ethynyl group by comparing the integrations of the signal at 2.53 ppm (signal a in **Fig. S2**) and proton signals of phenyl ring (signal i-m in **Fig. S2**). The coupling of the alkyne-$PC_{61}BAm$ and $AcMal_7$-N_3 was performed via the CuAAC click reaction in THF. The crude product was purified by passing through a neutral alumina column and precipitated into cold methanol to afford $AcMal_7$-C_{61} as brown solid in 58 % yield. The resulting product was well soluble in THF, chloroform, acetone, and *o*-dichlorobenzene and slightly soluble in toluene. ^1H NMR spectrum of the product showed characteristic signals assignable to the protons of $PC_{61}BAm$ and $AcMal_7$ (**Fig. S3**). The covalent attachment of the both moieties was confirmed by diffusion-ordered spectroscopy (DOSY), showing a single diffusion coefficient with $D = 3.8 \times 10^{-10}$ m^2 s^{-1} (**Fig. 3**). The absence of the characteristic IR band of the azide group at 2100 cm^{-1} indicates the completion of the reaction (**Fig. S4**). MALDI-TOF MS spectrometry provides further evidence of the successful formation of the $AcMal_7$-C_{61}. The most intense peak at *m*/*z* 3059.7 was assignable to the target compound with sodium ion $[M + Na]^+$ (**Fig. 4**).

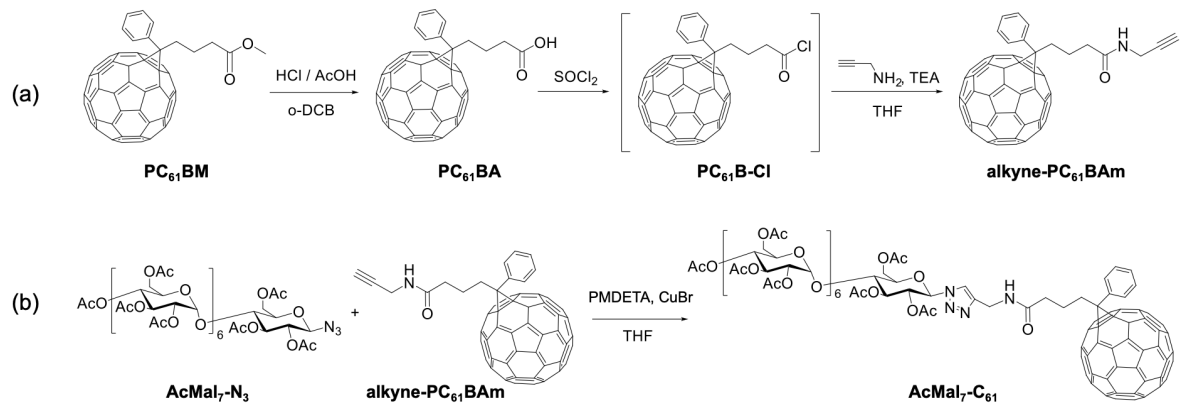

Scheme 2. Strategy used for the synthesis of $AcMal_7$-C_{61}: (a) Synthesis of alkyne-functionalized fullerene (alkyne-$PC_{61}BAm$) and (b) "Click" reaction of alkyne-$PC_{61}BAm$ with azide endo-functionalized paracetylated maltoheptaose ($AcMal_7$-N_3).

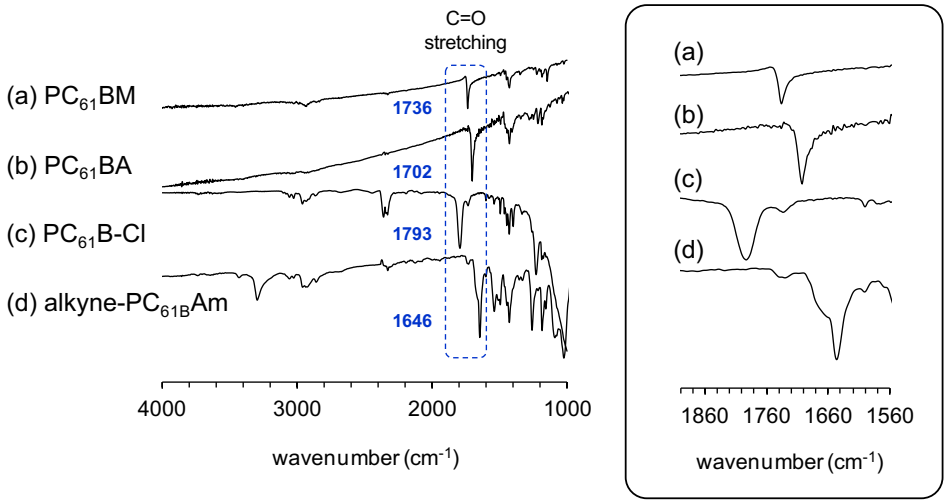

Fig. 2. FT-IR spectra of (a) $PC_{61}BM$, (b) $PC_{61}BA$, (c) $PC_{61}B$-Cl, and (d) alkyne-$PC_{61}BAm$.

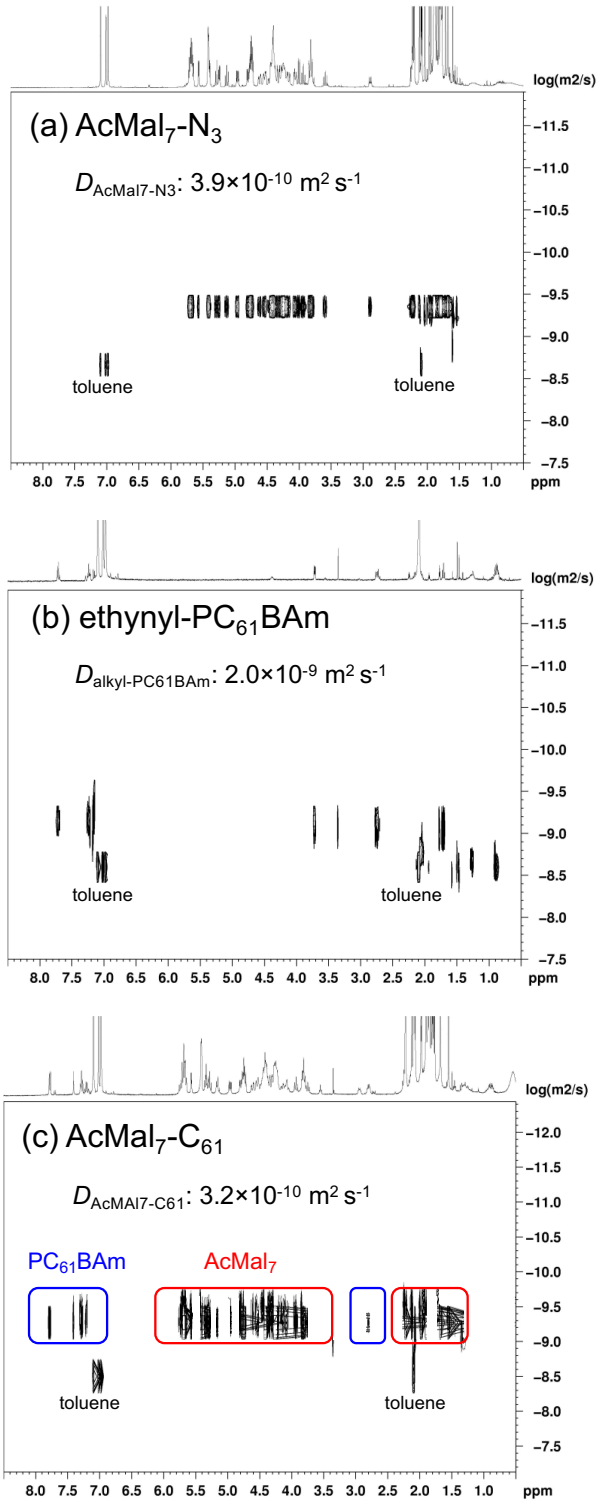

264

265 **Fig. 3**. ^{1}H-DOSY spectra of (a) AcMal$_7$-N$_3$, (b) alkyne-PC$_{61}$BAm, and (c) AcMal$_7$-C$_{61}$ in
266 toluene-d_8.

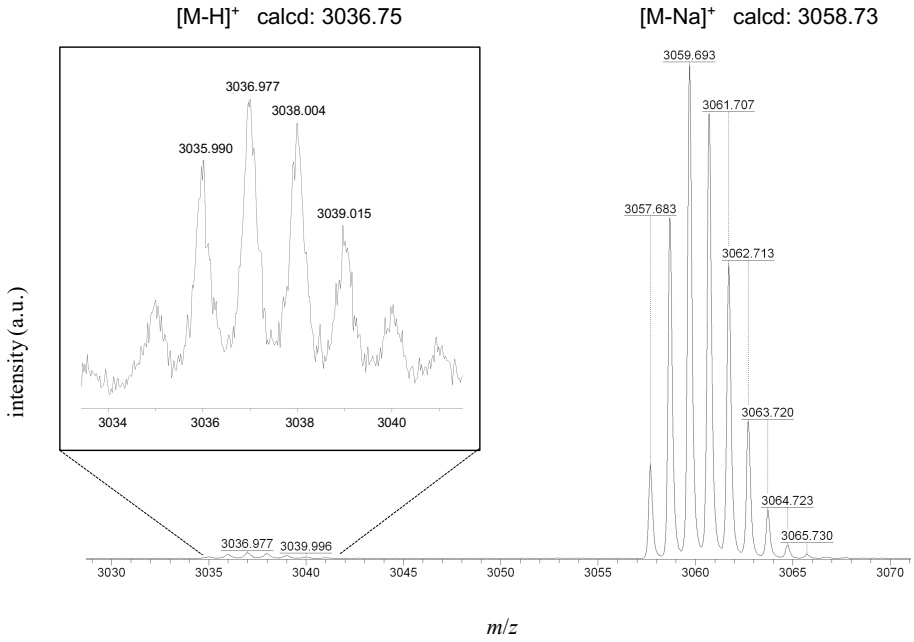

Fig. 4. MALDI-TOF MS spectrum of $AcMal_7$-C_{61} in positive mode.

3.3. Morphologies of P3HT-b-$AcMal_7$:$AcMal_7$-C_{61} blends

The morphology of the blend films consisting of the P3HT-*b*-$AcMal_7$ and $AcMal_7$-C_{61} with different donor(D):acceptor(A) composition ratio (w/w) was investigated by TEM. Note that the D:A ratio was calculated based on the total weight of the donor segments (*i.e.* P3HT) in the block copolymers with respect to that of acceptor moieties (*i.e.* fullerene) in the $AcMal_7$-C_{61}. All films were annealed at 210 °C for 10 min prior to the TEM observations to induce the microphase separation of the P3HT-*b*-$AcMal_7$. The TEM image of a thermally-annealed acceptor-free P3HT-*b*-$AcMal_7$ thin film showed a well-defined lamellar structure with a *d*-spacing of *ca.* 12 nm as reported previously (**Fig. 5a**) (Sakai-Otsuka et al., 2020). At 1:0.1 loading ratio, the blend film exhibited a periodic stripe pattern identical to that of the P3HT-*b*-$AcMal_7$ film, indicating that the $AcMal_7$-C_{61} at low concentration disturbed neither P3HT crystallization nor microphase separation of the P3HT-*b*-$AcMal_7$ (**Fig. 5b**). Electron diffraction (ED) pattern inserted in **Fig. 5b** also supports this fact by showing a sharp 0 2 0 reflection representing the π-stacking of the P3HT with a stacking period of ca. 3.8 Å. It is likely that the

$AcMal_7$-C_{61} molecules penetrate in the $AcMal_7$ domain of the phase-separated P3HT-*b*-$AcMal_7$ but are excluded from the P3HT domain without destroying the crystalline lamellar structure at this concentration. Upon increasing the D:A ratio up to 1:0.5, the diffraction pattern became less intense while the TEM image still showed the definite lamellar structures (**Fig. 5c**). At 1:1 D:A ratio, no distinctive ordered structure was observed, indicating that this system reached order-disordered transition (**Fig. 5d**). Nevertheless, the blend films of P3HT-*b*-$AcMal_7$:$AcMal_7$-C_{61} did not cause any crystallization of fullerene over the entire tested blend ratio range from 1:0.1 to 1:1 while a reference film of P3HT-*b*-$AcMal_7$:PCBM at 1:1 induced many PCBM aggregations after thermal annealing at 210 °C for 10 min (**Fig. S5**).

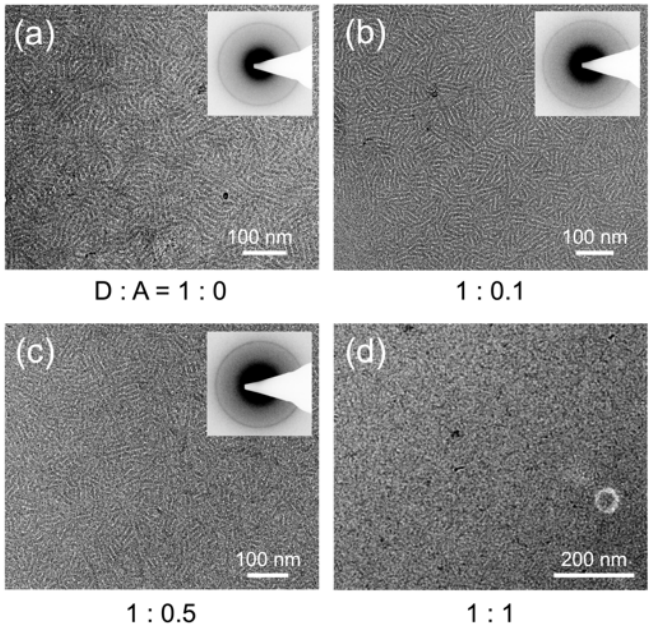

Fig. 5. TEM images of thermally annealed thin films of (a) P3HT-*b*-$AcMal_7$ and the blend of P3HT-*b*-$AcMal_7$ and $AcMal_7$-C_{61} with donor:acceptor ratio of (b) 1:0.1, (c) 1:0.5 and (d) 1:1 (annealing condition: 210 °C for 10 min). Insets: electron diffraction patterns of the corresponding film.

To assess the crystalline state of the P3HT and microscopic distribution of the $AcMal_7$-C_{61}, wide-angle X-ray scattering (WAXS) measurements were performed on the bulk samples of the P3HT-*b*-$AcMal_7$:$AcMal_7$-C_{61} blends together with that of individual components (single P3HT-*b*-$AcMal_7$ and $AcMal_7$-C_{61}). For all samples, *h* 0 0 and 0 2 0 reflections, corresponding

303 to the periodicity along the hexyl side chain direction and π-stacking periodicity, respectively,
304 are visible while their intensities decrease with increasing acceptor content (**Fig. 6**). This means
305 that the addition of the $AcMal_7$-C_{61} partially disrupts the crystallization of the P3HT segments.
306 A broad amorphous scattering originating from a short-range ordering of molecular
307 arrangement of the $AcMal_7$-C_{61} was observed in the WAXS profile of the $AcMal_7$-C_{61} (**Fig. 6e**)
308 and might be present underneath the WAXS profiles of the blend samples.
309 If the addition of the $AcMal_7$-C_{61} does not affect the crystalline structure of the P3HT
310 segments in the blend films, the scattering intensity should be expressed by a linear combination
311 of two reference WAXS profiles of single substances (P3HT-*b*-$AcMal_7$ (**Fig. 6a**) and $AcMal_7$-
312 C_{61} (**Fig. 6e**)) as illustrated in **Fig. S6**. For a weight fraction of P3HT-*b*-$AcMal_7$, α in the blend
313 system, the expected scattering intensity, I_{cal} is given as:

314 $$I_{cal} = \alpha I_{donor} + (1 - \alpha) I_{acceptor}$$

315 where I_{donor} and $I_{acceptor}$ are scattering intensities of the P3HT-*b*-$AcMal_7$ and $AcMal_7$-C_{61},
316 respectively. The comparison between experimental and calculated WAXS profiles was
317 presented in **Fig. 7**. The calculated profiles were normalized with respect to integrated area of
318 the corresponding WAXS profiles. At low 1:0.1 loading ratio, the calculated profile is almost
319 identical with the experimental one except for a slightly higher intensity of the 0 2 0 reflection.
320 At higher blend ratio, all peaks at *h* 0 0 and 0 2 0 of the combined profile became less prominent
321 compared to those of non-treated additive-free WAXS profile (**Fig. 6a**) as a consequence of the
322 superposition of non-negligible amorphous halo of the $AcMal_7$-C_{61}. Although the *h* 0 0 and 0 2
323 0 peaks in the experimental data are broader, indicating the smaller crystallite size of P3HT, we
324 can still recognize the crystalline nature of the P3HT segments. Hence, it is reasonable to
325 assume that the $AcMal_7$-C_{61} molecules are exclusively incorporated in the phase-separated
326 $AcMal_7$ nanodomains with limited deleterious effect on the initial lamellar morphology and
327 crystalline structure of the P3HT segments. Otherwise, the closely-packed P3HT crystalline
328 structure would not be maintained because of a bulkiness of the $AcMal_7$-C_{61} molecules. With

329 an adequate amount of the AcMal$_7$-C$_{61}$, the present P3HT-*b*-AcMal$_7$:AcMal$_7$-C$_{61}$ blend system
330 can provide a co-alternating D-A lamellar network at the exciton diffusion length scale, from
331 which we anticipate an improved photovoltaic performance despite the presence of the
332 insulating AcMal$_7$ segments in the blend.

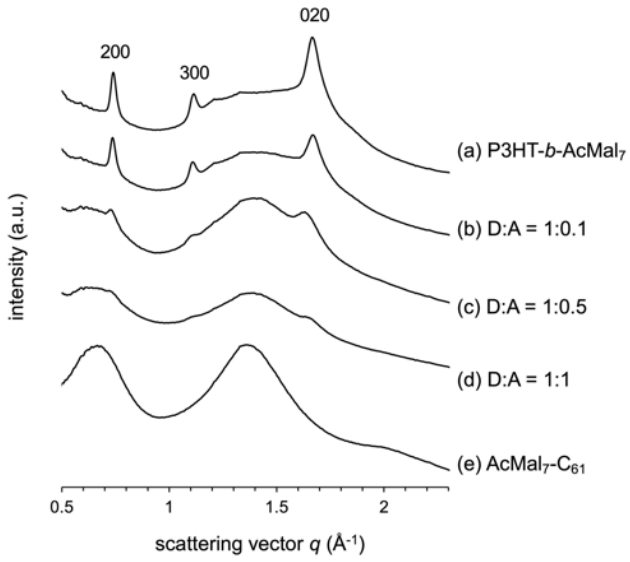

333

334 **Figure 6.** WAXS profiles of the thermally-annealed bulk samples of the single component of
335 (a) P3HT-*b*-AcMal$_7$ and (e) AcMal$_7$-C$_{61}$, and thermally-annealed bulk samples of the blend of
336 P3HT-*b*-AcMal$_7$ and AcMal$_7$-C$_{61}$ with a donor:acceptor ratio of (b) 1:0.1, (c) 1:0.5 and (d) 1:1
337 (annealing condition : 210 °C for 10 min).
338

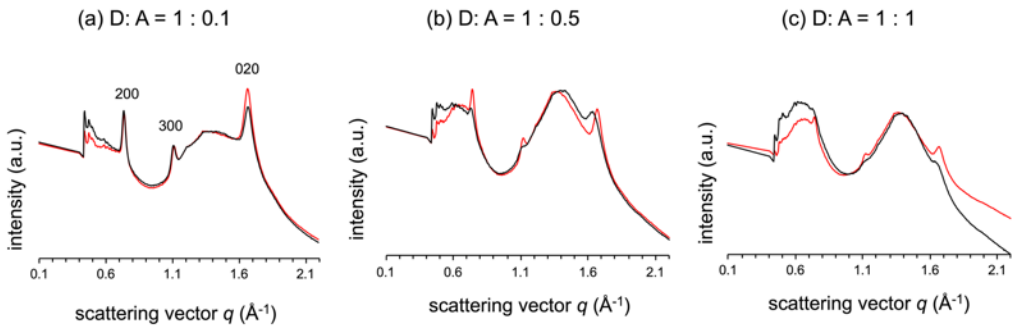

339

340 **Fig. 7.** Comparison between experimental WAXS profiles (black) and simulated profiles (red)
341 for the blends of P3HT-*b*-AcMal$_7$ and AcMal$_7$-C$_{61}$ with donor:acceptor ratio of (a) 1:0.1, (b)
342 1:0.5 and (c) 1:1.
343

4. Conclusion

We have demonstrated the well-defined D/A lamellar structures through a reciprocal self-organization of carbohydrate-*b*-P3HT block copolymer and a strategically designed carbohydrate-based fullerene derivative $AcMal_7$-C_{61}. The $AcMal_7$-C_{61} was synthesized via CuAAC "click" reaction of the alkyne-functionalized fullerene and azido-functionalized $AcMal_7$. The synthesized acceptor compound showed a good solubility in various organic solvents including THF, chloroform, acetone, and *o*-dichlorobenzene, which is advantageous for solution-based film fabrications. As expected from the different compatibility of $AcMal_7$-C_{61} to P3HT and $AcMal_7$, a morphological investigation of the blend system proved that the $AcMal_7$-C_{61} molecules are localized in the phase-separated $AcMal_7$ nanodomains upon annealing without causing the formation of fullerene crystals. The crystallinity of P3HT and well-defined lamellar morphology that were observed in the single P3HT-*b*-$AcMal_7$ film were retained up to 1:0.5 (D:A) blending ratio. This result indicates that the addition of newly designed $AcMal_7$-C_{61} to the highly-segregated P3HT-*b*-$AcMal_7$ block copolymer system could be a valuable approach to realize a conceptionally optimal D/A lamellar structures with sub-10 nm domain features, which ensures the effective exciton dissociation at the D/A interface. Additionally, cross-sectional TEM observation and GISAXS measurement revealed that the P3HT-*b*-$AcMal_7$ tends to spontaneously organize into perpendicularly-oriented lamellar structures relative to the film surface at the air/film interface while at the bottom interface the domain orientation depends on the nature of the substrate. This inherent nature of our high-χ block copolymer system would be industrially beneficial since no additional treatment, such as top-coat application, is required to control lamellar orientation at the top interface. The tuning of the microphase separation and investigation of charge carrier mobility of the ordered photoactive blend films are topics of future study.

Acknowledgements

R.B. acknowledges partial financial support from “SweetMemory” International France-Taiwan ANR project [#ANR-14-CE08-0021], Institute Carnot PolyNat ANR [#CARN-025-01] and the European Union’s Seventh Framework Program [FP7/2007-2013] under grant agreement n° 603519. This work was financially supported by the JSPS Grant-in-Aid for Scientific Research (B) [19H02769, T. S.], the Photoexcitonix Project (Hokkaido University, T. S.), and Creative Research Institute (CRIS, Hokkaido University, T. S.). The WOS was funded by the ANR under the "Investissements d'avenir" program [ANR-11-EQPX-0010]. R.B. would like to gratefully thank the CNRS and Grenoble Alpes University for partial financial support in this project, the Advanced Research Center for Green Materials Science and Technology, National Taiwan University (NTU) and Hokkaido University (Laboratory of Polymer Chemistry, Faculty of Engineering) for exchange students and fruitful collaboration.

Supporting Information

Supporting Information is available at: XXXXX.

References

Bates, C. M., Seshimo, T., Maher, M. J., Durand, W. J., Cushen, J. D., Dean, L. M., Willson, C. G. (2012). Polarity-Switching Top Coats Enable Orientation of Sub-10-nm Block Copolymer Domains. *Science*, *338*(6108), 775–779. https://doi.org/10.1126/science.1226046

Boudouris, B. W., Frisbie, C. D., & Hillmyer, M. A. (2008). Nanoporous Poly(3-alkylthiophene) Thin Films Generated from Block Copolymer Templates. *Macromolecules*, *41*(1), 67–75. https://doi.org/10.1021/ma071626d

Coakley, K. M., & McGehee, M. D. (2004). Conjugated Polymer Photovoltaic Cells. *Chemistry of Materials*, *16*(23), 4533–4542. https://doi.org/10.1021/cm049654n

Dou, L., You, J., Hong, Z., Xu, Z., Li, G., Street, R. A., & Yang, Y. (2013). 25th Anniversary Article: A Decade of Organic/Polymeric Photovoltaic Research. *Advanced Materials*, *25*(46), 6642–6671. https://doi.org/10.1002/adma.201302563

Hummelen, J. C., Knight, B. W., LePeq, F., Wudl, F., Yao, J., & Wilkins, C. L. (1995). Preparation and Characterization of Fulleroid and Methanofullerene Derivatives. *The Journal of Organic Chemistry*, *60*(3), 532–538. https://doi.org/10.1021/jo00108a012

Iovu, M. C., Zhang, R., Cooper, J. R., Smilgies, D. M., Javier, A. E., Sheina, E. E., Kowalewski, T., McCullough, R. D. (2007). Conducting Block Copolymers of Regioregular Poly(3-

hexylthiophene) and Poly(methacrylates): Electronic Materials with Variable Conductivities and Degrees of Interfibrillar Order. *Macromolecular Rapid Communications*, *28*(17), 1816–1824. https://doi.org/10.1002/marc.200700401

Lee, Y., & Gomez, E. D. (2015). Challenges and Opportunities in the Development of Conjugated Block Copolymers for Photovoltaics. *Macromolecules*, *48*(20), 7385–7395. https://doi.org/10.1021/acs.macromol.5b00112

Lin, Y., Lim, J. A., Wei, Q., Mannsfeld, S. C. B., Briseno, A. L., & Watkins, J. J. (2012). Cooperative Assembly of Hydrogen-Bonded Diblock Copolythiophene/Fullerene Blends for Photovoltaic Devices with Well-Defined Morphologies and Enhanced Stability. *Chemistry of Materials*, *24*(3), 622–632. https://doi.org/10.1021/cm203706h

Liu, J., Sheina, E., Kowalewski, T., & McCullough, R. D. (2002). Tuning the Electrical Conductivity and Self-Assembly of Regioregular Polythiophene by Block Copolymerization: Nanowire Morphologies in New Di- and Triblock Copolymers We gratefully acknowledge support from the NSF (CHE-9807707). *Angewandte Chemie International Edition*, *41*(2), 329. https://doi.org/10.1002/1521-3773(20020118)41:2<329::AID-ANIE329>3.0.CO;2-M

Miyanishi, S., Zhang, Y., Hashimoto, K., & Tajima, K. (2012). Controlled Synthesis of Fullerene-Attached Poly(3-alkylthiophene)-Based Copolymers for Rational Morphological Design in Polymer Photovoltaic Devices. *Macromolecules*, *45*(16), 6424–6437. https://doi.org/10.1021/ma300376m

Miyanishi, S., Zhang, Y., Tajima, K., & Hashimoto, K. (2010). Fullerene attached all-semiconducting diblock copolymers for stable single-component polymer solar cells. *Chemical Communications*, *46*(36), 6723. https://doi.org/10.1039/c0cc01819h

Sakai-Otsuka, Y., Nishiyama, Y., Putaux, J.-L., Brinkmann, M., Satoh, T., Chen, W.-C., & Borsali, R. (2020). Competing Molecular Packing of Blocks in a Lamella-Forming Carbohydrate- block -poly(3-hexylthiophene) Copolymer. *Macromolecules*, in press. https://doi.org/10.1021/acs.macromol.0c01801

Sakai-Otsuka, Y., Zaioncz, S., Otsuka, I., Halila, S., Rannou, P., & Borsali, R. (2017). Self-Assembly of Carbohydrate- block -Poly(3-hexylthiophene) Diblock Copolymers into Sub-10 nm Scale Lamellar Structures. *Macromolecules*, *50*(8), 3365–3376. https://doi.org/10.1021/acs.macromol.7b00118

Sary, N., Richard, F., Brochon, C., Leclerc, N., Lévêque, P., Audinot, J.-N., Berson, S., Heiser, T., Hadziioannou, G., Mezzenga, R. (2010). A New Supramolecular Route for Using Rod-Coil Block Copolymers in Photovoltaic Applications. *Advanced Materials*, *22*(6), 763–768. https://doi.org/10.1002/adma.200902645

Segalman, R. A., McCulloch, B., Kirmayer, S., & Urban, J. J. (2009). Block Copolymers for Organic Optoelectronics. *Macromolecules*, *42*(23), 9205–9216. https://doi.org/10.1021/ma901350w

Shah, M., & Ganesan, V. (2010). Correlations between Morphologies and Photovoltaic Properties of Rod−Coil Block Copolymers. *Macromolecules*, *43*(1), 543–552. https://doi.org/10.1021/ma9020467

Yu, G., Gao, J., Hummelen, J. C., Wudl, F., & Heeger, A. J. (1995). Polymer photovoltaic cells: Enhanced efficiencies via a network of internal donor-acceptor heterojunctions. *Science*, *270*(5243), 1789. https://doi.org/10.1126/science.270.5243.1789

Zhang, J., Clark, M. B., Wu, C., Li, M., Trefonas, P., & Hustad, P. D. (2016). Orientation Control in Thin Films of a High-χ Block Copolymer with a Surface Active Embedded Neutral Layer. *Nano Letters*, *16*(1), 728–735. https://doi.org/10.1021/acs.nanolett.5b04602

A carbohydrate-based fullerene derivative is designed, synthesized and applied to a lamellar-forming high-χ block copolymer system to realize an ordered donor/acceptor (D/A) network. A well-defined D/A lamellar structure of the blend with sub-10 nm domain features, which ensures the effective exciton dissociation at the D/A interface, is achieved upon thermal annealing.